Materials Transactions, Vol. 45, No. 7 (2004) pp. 2144 to 2149
Special Issue on Grain Boundaries, Interfaces, Defects and Localized Quantum Structures in Ceramics

Grain Boundary Energy and Tensile Ductility in Superplastic Cation-doped TZP

Akihide Kuwabara[1,*1], Syu Yokota[1,*2], Yuichi Ikuhara[2] and Taketo Sakuma[3]

[1]*Department of Materials Science, School of Engineering, The University of Tokyo, Tokyo 113-8656, Japan.*
[2]*Institute of Engineering Innovation, School of Engineering, The University of Tokyo, Tokyo 113-8656, Japan.*
[3]*Department of Advanced Materials Science, Graduate School of Frontier Sciences, The University of Tokyo, Tokyo 113-8656, Japan.*

Fine-grained 3Y-TZP has been known to show high superplasticity. Addition of a small amount of metal oxide influences the superplastic behavior in 3Y-TZP. In this study, 3Y-TZP doped with 1 mol% GeO_2, TiO_2 or BaO were fabricated, and respective grain boundary energy has been systematically measured by a thermal grooving technique with atomic force microscopy. It has been found that addition of Ge^{4+} or Ti^{4+} ions decreases the grain boundary energy to stabilize the grain boundaries in TZP whereas doping of Ba^{2+} ion increases the grain boundary energy to destabilize the grain boundaries. A change in the grain boundary energy should be due to segregation of dopant at grain boundaries. It has been also found that the elongation to failure of cation-doped 3Y-TZP is directly proportional to the stability of grain boundary. Grain boundary energy is thus one of the principal factors to determine the tensile ductility of TZP. In order to reveal the effect of dopant on the grain boundary energy, lattice static calculations and first principles molecular orbital calculations have been performed for supercells and model clusters including the present dopant, respectively. A series of results shows that substitution of Ge^{4+} or Ti^{4+} ion for Zr^{4+} ion increases the covalency of TZP, but the covalency of TZP is reduced by addition of Ba^{2+} ions. The grain boundary energy is found to have a relationship with covalency nearby grain boundaries in TZP.

(Received February 2, 2004; Accepted June 11, 2004)

Keywords: *tetragonal zirconia polycrystal, superplasticity, grain boundary energy, first principles calculation*

1. Introduction

Superplasticity in fine-grained ceramics has been widely examined for many years. Tetragonal zirconia polycrystal (TZP) with submicrometer grain size shows high superplasticity at temperatures above 1573 K.[1–4] Especially, yttria-stabilized TZP (Y-TZP) exhibits excellent superplasticity, and an elongation to failure of 800% has been obtained at an initial strain rate of $2.7 \times 10^{-4}\,s^{-1}$ and 1823 K for 3-mol%-yttria-stabilized TZP (3Y-TZP).[2] Several studies have been made to examine the effect of oxide doping on the superplasticity of Y-TZP. For instance, addition of 5 wt% TiO_2 into 2.5Y-TZP enhances tensile ductility, an elongation to failure of 382% at an initial strain rate of $1.3 \times 10^{-4}\,s^{-1}$ and 1673 K.[5] A similar effect has been observed in 1 mol%-GeO_2-doped 2.5Y-TZP.[6]

Many discussions have been made to clarify factors which determine the tensile ductility of superplastic ceramics. Kim *et al.*[7] presented that an elongation to failure in ceramics should be expressed as a function of flow stress and the fracture energy of grain boundary. Mimurada *et al.*[8] systematically examined the superplastic deformation behavior of 3Y-TZP doped with various types of metal oxides, and found that the tensile ductility of 3Y-TZP increases with the reduction of flow stress. On the other hand, it has been reported that the ductility of SiO_2-doped TZP cannot be explained only from flow stress.[9–11] Recent studies have pointed out that covalent bonding states nearby grain boundaries correlate with the tensile ductility of TZP and Al_2O_3.[12–14] Further analyses to the grain boundaries are indispensable to fully understand the tensile ductility of TZP.

The aim of this paper is to investigate the tensile ductility of 3Y-TZP from the viewpoints of grain boundary energy and a chemical bonding state around a grain boundary. In order to obtain a chemical bonding state including the effect of lattice relaxation, a lattice static calculation and a molecular orbital calculation were combined.

2. Experimental Procedure

Commercially available 3Y-TZP high-purity powder (Tosoh Co., Ltd., Tokyo, Japan) was used as starting material. 3Y-TZP was doped with 1 mol% cation. Dopant oxides are germanium oxide (Rare Metallics Co., Ltd., Tokyo, Japan), titanium oxide (Sumitomo Osaka Cement Co., Ltd., Osaka, Japan), and barium oxide (Soekawa Chemical Co., Ltd., Tokyo, Japan). 3Y-TZP powders were mixed with dopant oxide powders by ball-milling in ethanol for 24 h and dried in Ar atmosphere. Subsequently, the powders were sieved to $<200\,\mu m$. The resulting powders were uniaxially pressed into a bar at 33 MPa and then pressed by cold isostatic press (CIP) in a rubber tube under a pressure of 100 MPa. Green bodies were sintered at 1623 or 1673 K for 2 h in air so as to have the same grain size. The relative densities for the sintered samples were more than 98%. A single tetragonal phase was observed to form in the all samples from X-ray diffraction analyses. Microstructure observation was conducted with scanning electron microscopy (SEM) (JSM-5200, JEOL Ltd., Tokyo, Japan). Grain size was measured by a linear intercept method from SEM micrographs, and average grain size was determined to be about 0.4 μm for all samples.

Grain boundary energy was measured by a conventional thermal grooving technique. Firstly, a surface of the sintered samples was polished with 9 μm, 3 μm, and 1 μm diamond suspensions to achieve a mirror state. The polished samples were then annealed in air at 1473 K, 1573 K, and 1673 K for

*[1]Present address: Department of materials Science and Engineering, Kyoto University, Kyoto 606-8501, Japan.
*[2]Graduate Student, The University of Tokyo. Present address: Hewlett-Packard Japan, Ltd. Tokyo 140-8641, Japan.

60 min, 30 min, and 15 min, respectively. Dihedral angles at grain boundaries were directly measured from the groove profiles obtained by atomic force microscopy (AFM) (SPM-9500E, Shimadzu Co., Kyoto, Japan). Measurements of dihedral angles were carried out at 120 different points in each sample.

3. Computational Procedure

3.1 Lattice static calculation

Lattice static calculations have been conducted employing the computer code, GULP.[15] A lattice energy is described by a long-range Madelung potential and a short-range Buckingham potential with parameters reported by two groups, Lewis and Catlow,[16] and Dwibedi and Cormack.[17] The structural parameters of t-ZrO_2 unit cell obtained by GULP are listed in Table 1. As shown in the table, the calculated parammeters are in good agreement with the experimental values. A supercell containing 108 t-ZrO_2 formula units was constructed for the model of 3Y-TZP using the unit cell. Four Y^{3+} ions and two O^{2-} vacancies were introduced into the supercell. An atomic configuration around Y^{3+} ions and O^{2-} vacancies is illustrated in Fig. 1. Each O^{2-} vacancy was located at a mutual second nearest neighbor site from two Y^{3+} ions.[18–22] At this low dopant content, tetragonal phase is not stable yet. Therefore, structure optimization for the 3Y-TZP model was limited in spherical areas containing of the nearest neighbor anion sites from dopant and vacancy sites. The dimensions of supercell were fixed. The initial structures of the supercells for cation-doped TZP were the same as that of the optimized 3Y-TZP supercell. Dopant was substituted for the $Zr_{(1)}$ site indicated by an arrow in Fig. 1. When a Ba^{2+} ion is substituted for a Zr^{4+} ion, an O^{2-} vacancy is further introduced at the second nearest neighbor site from Ba^{2+} ions. In the calculations for cation-doped TZP, structure optimization was limited to the nearest neighbor anions from substituted dopant. Table 2 shows average bond length between a cation and an O^{2-} ions in the optimized structures. Calculated bond length reflects the ionic size of cation. This implys that the effect of ionic size on atomic structures are taken into account in our calculations.

Table 1 Theoretical and experimental structural parameters of t-ZrO_2.

	a/nm	c/nm	d_z
This work	0.3588	0.5216	0.060
Exp.[32]	0.3591	0.5169	0.046

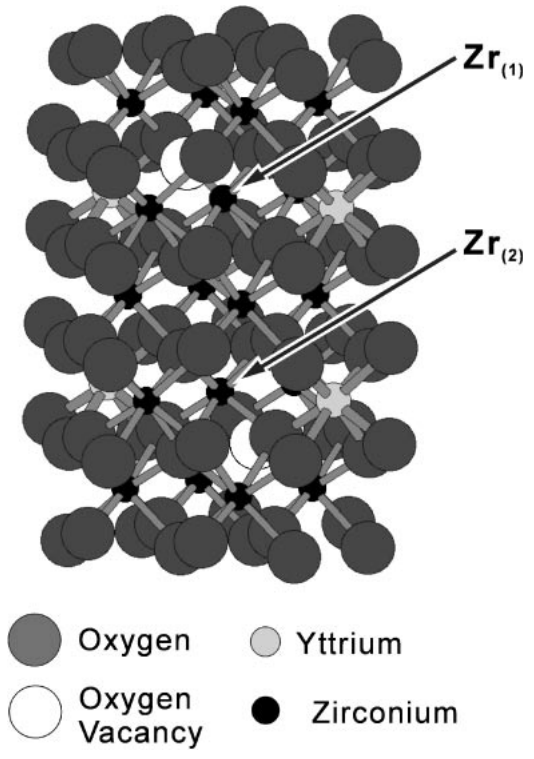

Fig. 1 An atomic configuration around Y^{3+} ions and O^{2-} vacancies in the calculation for 3Y-TZP. A model cluster of 3Y-TZP in a DV-Xα molecular orbital calculation has the same structure.

Table 2 Average optimized bond length between cations and O^{2-} ions in t-ZrO_2.

Type	Bond length, L/nm	Ionic radius,[33] r/nm
Zr	0.221	0.084
Ge	0.207	0.053
Ti	0.212	0.074
Ba	0.242	0.142

3.2 First principles molecular orbital calculation

Electronic structures were calculated by the discrete variational (DV)-Xα method[23] employing the computer code of SCAT.[24] In this method, the electronic structure of a model cluster is obtained self-consistently by solving one-electron Schlödinger equations. Molecular orbitals (MOs) are represented by a linear combination of atomic orbitals. The atomic orbitals are numerically obtained by solving radial part of a Schlödinger equation for each atom. Atomic charge density is renewed using atomic orbital populations in the molecular orbitals by the Mulliken population analysis[25] at each iteration until it becomes self-consistent. Therefore, the atomic basis functions are optimized under given chemical conditions. 1s-2p for oxgen, 1s-5p for zirconium, 1s-5p for yttrium, 1s-6s for barium, 1s-4p for titanium and 1s-4p for germanium were sufficient to reproduce core and valence states in GeO_2-doped, TiO_2-doped, and BaO-doped 3Y-TZP. In addition, bond overlap population (BOP), strength of covalent bonding, was calculated using the Mulliken population analysis.

The structure of $(Y_4Zr_{18}O_{86})^{88-}$ cluster used for a calculation to 3Y-TZP is shown in Fig. 1. This cluster is composed of 108 ions and includes up to the sixth-nearest neighbor oxygen ions from the $Zr_{(1)}$ and $Zr_{(2)}$ sites indicated by arrows in Fig. 1. $(GeY_4Zr_{17}O_{86})^{88-}$ (3Y-1Ge) and $(TiY_4Zr_{17}O_{86})^{88-}$ (3Y-1Ti) clusters were constructed for calculations of GeO_2-doped TZP and TiO_2-doped TZP, respectively. $(BaY_4Zr_{17}O_{85})^{88-}$ (3Y-1Ba) clusters were made as a model cluster of BaO-doped 3Y-TZP. A cluster was put into a field of Madelung potential composed of about 6000 point charges. All model clusters were constructed

using optimum atomic positioins obtained from the calculations for doped and undoped 3Y-TZP supercells using GULP code.

4. Result and Discussion

4.1 Grain boundary energy and tensile ductility in doped TZP

Figure 2 shows an AFM image of undoped 3Y-TZP annealed at 1673 K. As shown in the figure, Grain boundaries have been thermally grooved, and equiaxial grains are clearly observed. All samples in the present study show similar microstructures. Figure 3 indicates the distributions of dihedral angles in the specimens annealed at 1673 K. The number of angles is counted at every 2.5°. As shown in the figure, distributing ranges of measured angles are about 20° in all samples. No sample has multipeak in the distribution. This tendency is consistent with the previous report on 8 mol%Y_2O_3-doped c-ZrO_2 polycrystal by Tsoga and Nikolopoulos.[26] Thermal grooving seems to have uniformly progressed at the grain boundaries in doped and undoped 3Y-TZP. Table 3 shows averages of groove angles measured in

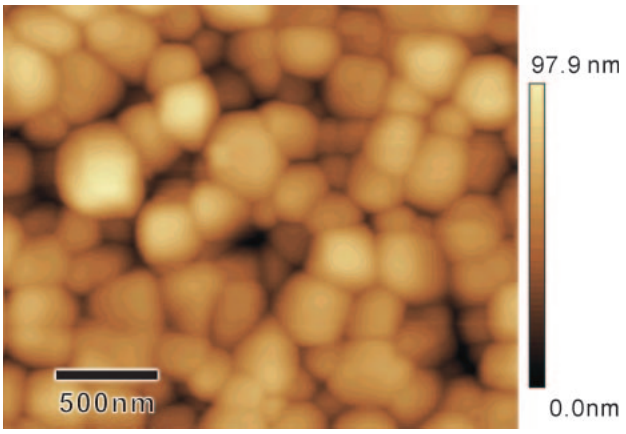

Fig. 2 An AFM image for the surface of 3Y-TZP annealed at 1673 K in air. A color bar to the right side of the image indicates the height of sampling point.

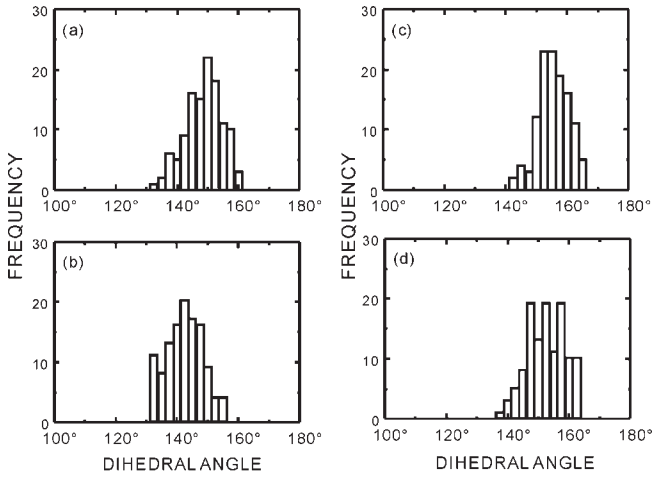

Fig. 3 Distribution of thermal grooved angles in the specimens annealed at 1673 K. (a) 3Y-TZP, (b) BaO-doped 3Y-TZP, (c) GeO_2-doped 3Y-TZP, and (d) TiO_2-doped 3Y-TZP.

Table 3 Average grooving angle in each specimen measured by AFM.

Specimen	Annealing temperature, T/K	Average groove angel
3Y-TZP	1473	140.46
	1573	144.26
	1673	147.50
GeO_2-doped 3Y-TZP	1473	146.22
	1573	151.09
	1673	154.27
TiO_2-doped 3Y-TZP	1473	144.16
	1573	148.76
	1673	151.39
BaO-doped 3Y-TZP	1473	132.34
	1573	137.43
	1673	141.27

doped and undoped TZP. The average angle is dependent on an annealing condition and a type of dopant. The average angles of 1 mol%BaO-doped 3Y-TZP are smaller than those of 3Y-TZP. On the contrary, GeO_2-doped 3Y-TZP and TiO_2-doped 3Y-TZP has larger average angles than 3Y-TZP. It has been reported that dopant cations are likely to segregate at grain boundaries in TZP.[10,11,27,28] The dependence of groove angle on dopant is supposed to result from segregation of dopant at grain boundaries.

Grain boundary energy (γ_{gb}) is expressed by surface energy (γ_s) and grooving angle at a grain boundary (ϕ) as follows,

$$\gamma_{gb} = 2\gamma_s \cos\left(\frac{\phi}{2}\right). \quad (1)$$

From this equation, we can define the normalized grain boundary energy (γ_{NGB}) by the following equation,

$$\gamma_{NGB} = \frac{\gamma_{gb}}{\gamma_s} = 2\cos\left(\frac{\phi}{2}\right). \quad (2)$$

The value of γ_{NGB} becomes smaller when grain boundary energy more decreases than surface energy. γ_{NGB} corresponds to the relative stability of a grain boundary to a surface and allows us to evaluate the stability of grain boundary without measurement of surface energy. Figure 4 shows a plot of γ_{NGB} against an annealing temperature, in

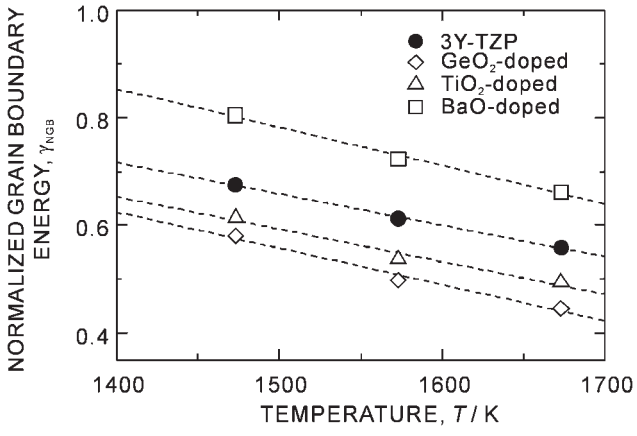

Fig. 4 A plot of γ_{NGB} of catioin-doped TZP against annealing temperature.

which γ_{NGB} has been calculated from an average dihedral angle in each sample shown in Table 2. GeO_2-doped 3Y-TZP and TiO_2-doped 3Y-TZP have smaller γ_{NGB} than 3Y-TZP. γ_{NGB} becomes larger by doping of Ba^{2+} ions. These tendencies are commonly observed in the temperature range of 1473 to 1673 K. It is implied that GeO_2 and TiO_2 stabilize the grain boundaries to reduce the grain boundary energy in 3Y-TZP, and that addition of BaO destabilizes the grain boundaries to increase the grain boundary energy in 3Y-TZP. Kim *et al.*[7] have proposed from the viewpoint of fracture mechanics that the true strain at failure (ε_f) of superplastic ceramics can be expressed by the following equation,

$$\varepsilon_f = \frac{1}{q}\ln\left[\frac{E\gamma_s(2-\gamma_{gb}/\gamma_s)}{\pi C_0 {\sigma_f}^2}\right], \quad (3)$$

where E is Young's modulus, C_0 is an initial cavity size, σ_f is fracture stress (almost the same as flow stress), and q is a material constant related to deformation mechanism. In the parameters of eq. (3), σ_f and γ_{gb}/γ_s, namely γ_{NGB}, should be mainly affected by doping. The eq. (3) suggests that reduction of flow stress enhances the tensile ductility. Mimurada *et al.*[8] have pointed out that reduction of flow stress is a factor to increase the tensile ductility of cation-doped TZP. This is in agreement with the eq. (3). In addition, reduction of γ_{NGB} is supposed to result in enhancement of ductility from the eq. (3). Figure 5 shows a plot of the ε_f of cation-doped TZP[8] against $\ln(2-\gamma_{NGB})$. The ε_f linearly increases with increase of $\ln(2-\gamma_{NGB})$. This means that elongation to failure become larger with stabilization of grain boundary. Our result is also consistent with the eq. (3). The tensile ductility of cation-doped TZP is probably affected not only by flow stress but also by stabilization of grain boundary. The ductility of superplastic ceramics has been mainly discussed from the viewpoint of flow stress thus far. It should be noted that the tensile ductility of cation-doped TZP correlates with the stability of grain boundary as well as the flow stress.

4.2 Chemical bonding state of doped TZP

Observations of grooving angle by means of AFM have revealed that grain boundary energy changes with the variation of dopant. This is supposed to result from a change

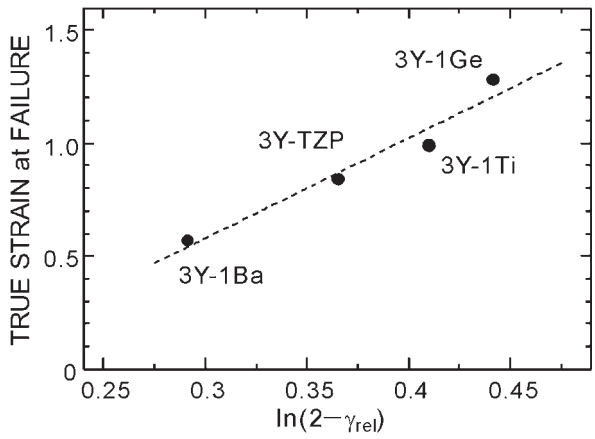

Fig. 5 A plot of the elongation to failure for various cation-doped TZP[8] against $\ln(2-\gamma_{NGB})$.

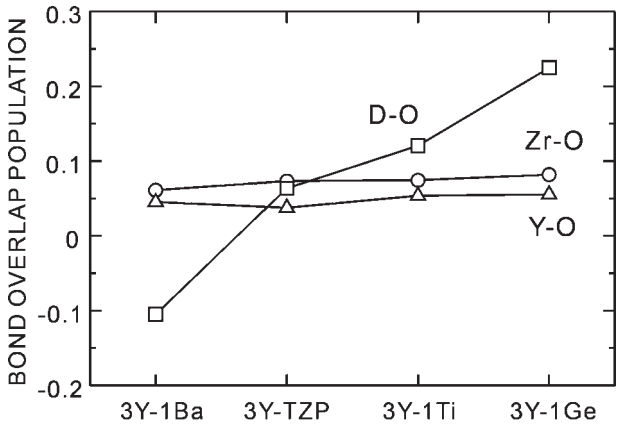

Fig. 6 Bond overlap population of Zr-O, Y-O, and dopant(D)-O bonds in each model cluster.

in the chemical bonding states nearby grain boundaries attributed to segregation of dopant. Wu *et al.*[29–31] calculated the effects of impurity atoms on grain boundary energy in iron using Full-potential Linear Augmented Plane-Wave (FLAPW) calculation. They have proposed that covalent interaction across grain boundary determines the difference of grain boundary energy and surface energy, namely fracture energy, in iron and that the covalent interaction is sensitive to the segregation of impurity. Based on this report, we focused on the influence of the segregated dopant on a covalent bonding state in TZP.

Covalency can be quantitatively analyzed with a parameter of BOP, which is calculated from the Mulliken population analysis.[25] Figure 6 indicates the BOP of Zr-O, Y-O, and dopant (D)-O bonds in undoped and doped TZP clusters. The covalency of D-O bond obviously depends on the type of dopant. The BOPs of Ge-O and Ti-O bonds are larger than that of a Zr-O bond. These dopants form more covalent bonds with neighboring oxygen than Zr-O bonds. On the contrary, the BOP of a Ba-O bond is negative. This means that a Ba-O bond is in an anti-bonding state and energetically unstable. The BOPs of Zr-O and Y-O bonds are almost constant among the all clusters. The substituting dopants influence on localized chemical bonding states around themselves. An overlap population diagram (OPD) enables us to analyze a change in a covalent bonding state in detail. Figure 7 shows OPDs of D-O bonds in cation-doped 3Y-TZP clusters. As a reference, an OPD of a Zr-O bond in 3Y-TZP cluster is also indicated in Fig. 7. The highest occupied molecular orbital (HOMO) level is set to be 0 eV in each cluster. Bonding and anti-bonding components of the Zr-O bond at 0 to −5 eV are attributed to the hybridization of Zr4d-O2p. The Ge-O bond has large bonding components from Ge4s-O2p and Ge4p-O2p at higher energy levels in valence bands. The bonding components of the Ti-O bond nearby HOMO are due to Ti3d-O2p and Ti4s-O2p. The Ge-O and Ti-O bonds have larger bonding components than the Zr-O bond. The Zr-O bond has anti-bonding components in valence bands, whereas the Ge-O and Ti-O bonds have slight anti-bonding components. These lead to that the covalency of the Ge-O and Ti-O bonds is higher than that of the Zr-O bond. A Ba-O bond has very large anti-bonding components of Ba5p-O2p and Ba5d-O2p

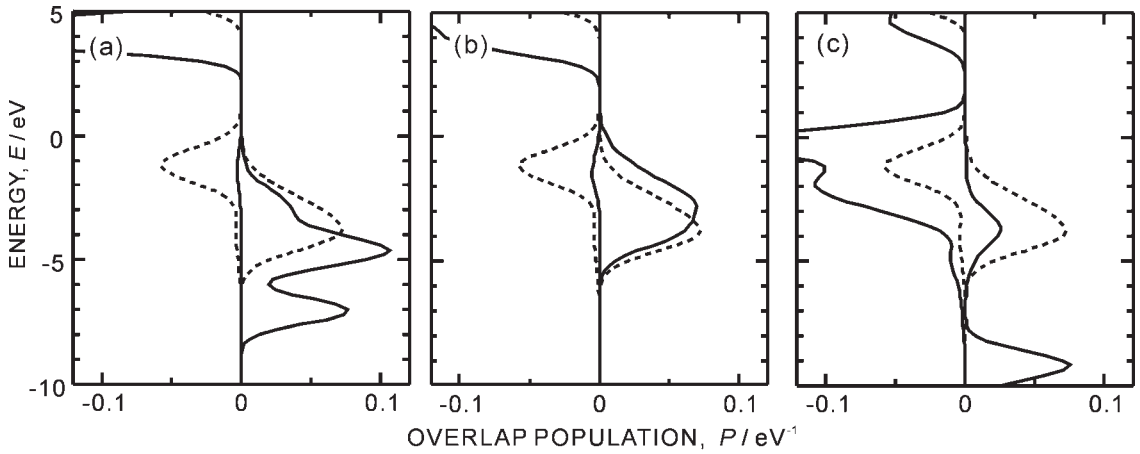

Fig. 7 Overlap population diagrams of the dopant-O bond in (a) 3Y-1Ge, (b) 3Y-1Ti, and (c) 3Y-1Ba clusters. For comparison, the overlap population diagram of $Zr_{(1)}$-O bonds in 3Y-TZP cluster is also indicated by dashed lines.

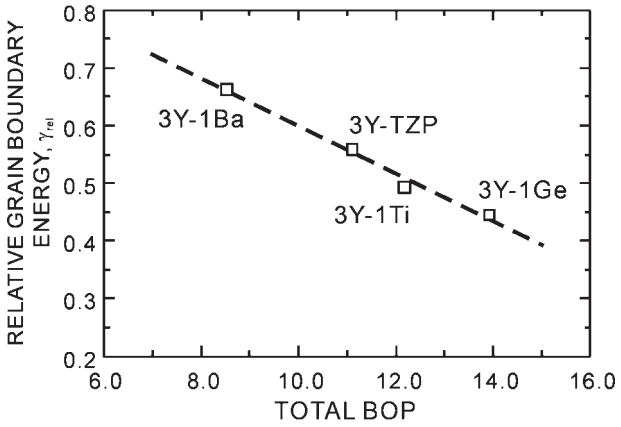

Fig. 8 A plot of γ_{NGB} against the total bond overlap population of cation-doped 3Y-TZP cluster.

in higher valence bands. The negative BOP of the Ba-O bond is originated from the anti-bonding components.

Our calculations show that a covalent bonding state around substituting dopant is clearly different from that of a Zr-O bond. As mentioned before, dopants are likely to segregate to grain boundaries in TZP.[10,11,27,28] The segregated dopant probably changes the covalent bonding state nearby grain boundaries. Effective covalency can be evaluated using total BOP of all bonds in a cluster. Figure 8 shows γ_{NGB} plotted against a total BOP. It is clearly shown that the stability of grain boundaries increases with increasing of covalency in cation-doped TZP systems. Wu *et al.*[29–31] reported that higher covalent interaction between segregated impurity and iron atoms increases the cohesion of grain boundaries in iron. Similarly, stabilization of grain boundaries in GeO_2-doped TZP and TiO_2-doped TZP should be attributed to increasing of covalency at grain boundaries with segregation. The grain boundaries of BaO-doped TZP should be destabilized by the formation of anti-bonding Ba-O bonds.

5. Conclusion

The grain boundary energy of 3Y-TZP doped with 1 mol% GeO_2, TiO_2 or BaO were measured by a thermal grooving technique. The grain boundary energy of cation-doped TZP depends on the type of dopant. Elongation to failure are improved by stabilization of grain boundary compared to surface. This is consistent with the model proposed by Kim *et al.*,[8] which suggests the dependence of tensile ductility on the fracture energy of grain boundary. The tensile ductility of TZP can be discussed not only from flow stress but also from the stability of grain boundary. Our first principles molecular orbital calculations have clarified that stabilization of a grain boundary is related to strong covalent interaction between segregated dopants, such as Ge^{4+} and Ti^{4+} ions, and O^{2-} ions. On the other hand, a grain boundary becomes unstable owing to segregation of Ba^{2+} ions which form an anti-bonding state. The present study indicates that superplasticity of TZP controlled by a chemical bonding state at a grain boundary.

Acknowledgements

This work was financially supported by a Grant-in-Aid for Scientific Research on Priority Areas (No. 751) from the Ministry of Education, Culture, Sports, Science and Technology, Japan. A part of this work was also supported by a grant-in-aid for Japan Society for the Promotion of Science Fellows (14-08214) from the Ministry of Education, Science, Sports and Culture, Japan.

REFERENCES

1) F. Wakai, S. Sakaguchi and Y. Matsuno: Adv. Ceram. Mater **1** (1986) 259.
2) T. G. Nieh and J. Wadsworth: Acta Metall. Mater. **38** (1990) 1121–1133.
3) D. J. Schissler, A. H. Chokshi, T. G. Nieh and J. Wadsworth: Acta Metall. Mater. **39** (1991) 3227–3236.
4) A. Lakki, R. Scaller, M. Neuer and C. Carry: Acta Metall. Mater. **41** (1993) 2845–2853.
5) K. Tsurui and T. Sakuma: Scr. Mater. **4** (1996) 443–447.
6) J. Mimurada, T. Kondo, Y. Takigawa, Y. Ikuhara and T. Sakuma: Mater. Sci. Forum **304–306** (1999) 543–548.
7) W.-J. Kim, J. Wolfenstine and O. D. Sherby: Acta Metall. Mater. **39** (1991) 199–208.
8) J. Mimurada, M. Nakano, K. Shimura, K. Sasaki, Y. Ikuhara and T. Sakuma: J. Am. Ceram. Soc. **84** (2001) 1817–1821.

9) Y. Ikuhara, K. Sasaki, P. Thavorniti and T. Sakuma: The Third Pacific Rim International Conference on Advanced Materials and Proceeding (PRICM3) Edited by M. A. Imam, R. denale, S. Hanada, Z. Zhong and D. N. Lee (1998) 1747–1754.
10) Y. Ikuhara, P. Thavorniti and T. Sakuma: Acta Mater. **45** (1997) 5275–5284.
11) P. Thavorniti, Y. Ikuhara and T. Sakuma: J. Am. Ceram. Soc. **81** (1998) 2927–2932.
12) H. Yoshida, Y. Takigawa, Y. ikuhara and T. Sakuma: Mater. Trans. **43** (2002) 1566–1572.
13) A. Kuwabara, S. Yokota, Y. Ikuhara and T. Sakuma: Mater. Trans. **43** (2002) 2468–2472.
14) P. H. Imamura, N. D. Evans, T. Sakuma and M L. Mecartney: J. Am. Ceram. Soc. **83** (2000) 3095–3099.
15) J. D. Gale: J. Chem. Soc. Faraday Trans. **93** (1997) 629.
16) A. Dwivedi and A. N. Cormack: Phil. Mag. A **61** (1990) 1–22.
17) G. V. Lewis and C. R. A. Catlow: J. Phys. C: Solid State Phys. **18** (1985) 1149–1161.
18) P. Li, I-W. Chen and J. E. P. Hahn: J. Am. Ceram. Soc. **77** (1994) 118–128.
19) M. O. Zacate, L. Minervini, D. J. Bradfield, R. W. Grimes and K. E. Sickafus: Solid State Ionics **128** (2000) 243–254.
20) M. S. Khan, M. S. Islam and D. R. Bates: J. Mater. Chem. **8** (1998) 2299–2307.
21) G. Stapper, M. Bernasconi, N. Nicoloso and M. Parrinello: Phys. Rev. B **59** (1999) 797–810.
22) A. Bogicevic, C. Wolverton, G. M. Crosbie and E. B. Stechel: Phys. Rev. B **64** (2001) 014106.
23) D. E. Ellis, H. Adachi and F. W. Averill: Surf. Sci. **58** (1976) 497.
24) H. Adachi, M. Tsukada and C. Satoko: J. Phys. Soc. Jpn. **45** (1978) 875–883.
25) R. S. Mulliken: J. Chem. Phys. **23** (1955) 1833.
26) A. Tsoga and P. Nikolopoulos: J. Mater. Sci. **31** (1996) 5409–5413.
27) J. Mimurada, K. Sasaki, Y. Ikuhara and T. Sakuma: Key Engineering Materials **171–174** (2000), 383–388.
28) K. Nakatani, H. Nagayama, H. Yoshida, T. Yamamoto and T. Sakuma: Scr. Mater. **49** (2003) 791–795.
29) R. Wu and A. J. Freeman: Science **265** (1994) 376–380.
30) R. Wu and A. J. Freeman: Phys. Rev. B **50** (1994) 75–81.
31) R. Wu and A. J. Freeman: Phys. Rev. B **53** (1996) 7504–7509.
32) N. Igawa, Y. Ishii, T. Nagasaki, Y. Morii, S. Funahashi and H. Ohno: J. Am. Ceram. Soc. **76** (1993) 2673–2676.
33) R. D. Shanon: Acta. Cryst. **A32** (1976) 751–767.